Journal of Asian Earth Sciences 187 (2020) 104098

Contents lists available at ScienceDirect

Journal of Asian Earth Sciences

journal homepage: www.elsevier.com/locate/jseaes

Determination of the isostatic and gravity Moho in the East China Sea and its implications

Songbai Xuan[a,b,c], Shuanggen Jin[a,d,*], Yong Chen[b]

[a] School of Remote Sensing and Geomatics Engineering, Nanjing University of Information Science and Technology, Nanjing 210044, China
[b] Nanjing Longyuan Microelectronic Co., LTD, Nanjing 211106, China
[c] Laurel Geophysical Instruments Limited, Shanghai 200232, China
[d] Shanghai Astronomical Observatory, Chinese Academy of Sciences, Shanghai 200030, China

ARTICLE INFO

Keywords:
Isostatic Moho
Gravity Moho
Subduction zone
East China Sea

ABSTRACT

The East China Sea (ECS) is located among the Eurasian, Pacific and Philippine Sea plates, whose crustal structure and evolution are very complex. Elevation, geoid and gravity anomaly data are used in this study to determine the isostatic and gravity Moho topography of the ECS and surroundings. The gravity effects of sediments and subducting slabs are computed using recent datasets during estimation of the gravity Moho, and the results show good agreement between the gravity Moho and seismic results. The crustal isostatic implications of the difference between the isostatic and gravity Moho are discussed, and the decreasing Moho depth from the coast of the mainland China to the western margin of the Okinawa Trough suggests continental crust-type features, similar to the Yellow Sea. A combined isostatic analysis, which takes the difference between the isostatic and gravity Moho into account, indicates that the shallower Moho beneath the Okinawa Trough and the depressed Moho beneath the Ryukyu Arc may have implications for rifting in the Okinawa Trough. The steep Moho along the Ryukyu Trench marks the continent-ocean boundary at the crustal scale, which is consistent with the subduction of the Philippine Sea Plate. Taking the eastward extension of the ECS into account, it is expected that this would be steeper if it was generated by the isostatic over- and under-compensation beneath the Ryukyu Arc and Trench, respectively.

1. Introduction

The East China Sea (ECS) is an eastern marginal oceanic basin of the Eurasian continent (Jin et al., 2007; Xu et al., 2014; Suo et al., 2015). From west to east, it consists of the Zhe-Min uplift Belt (ZB), Continental shelf Basin (CB), Diaoyudao uplift Belt (DB) and Okinawa Trough (Fig. 1). The tectonic structure of, and around, the ECS includes troughs, trenches, basins and sea-mount, and is therefore complex. The region records a protracted tectonic evolutionary history (Yu and Chow, 1997; Xu et al., 2014; Suo et al., 2015; Ding et al., 2017). Several geodynamic models have been proposed to interpret the evolution of the ECS, such as the subduction of the Philippine Sea Plate (Ding et al., 2017; Shang et al., 2017) and rifting of the ECS (Kimura, 1985; Sibuet et al., 1998; Li et al., 2012; Xu et al., 2014).

Multiple geophysical technologies have been applied to determine the crustal structure and investigate the evolution of the ECS (Ludwig et al., 1973; Feng et al., 1993; Harabaglia and Doglioni, 1998; Nakamura et al., 2003; Gao et al., 2006; Hao et al., 2006; Shang et al., 2017), especially the Moho topography (Hao et al., 2006; Ding et al., 2017; Guan et al., 2019). The Moho topography, which is an interface with high wave-speeds and large density contrasts, provides significant knowledge of the lithospheric structure (Thybo et al., 2013). As such, the gravity-derived Moho, which is relatively inexpensive to obtain, is now widely considered as an effective and indispensable tool, and can be used to obtain information on submarine structures (Tiberi et al., 2001; Fullea et al., 2006; Bai et al., 2014; Autin et al., 2016). Several previous studies suggest that the Moho depth in the ECS and Yellow Sea is in the 25–30 km (Gao et al., 2006; Hao et al., 2006; Choi et al., 2015; Ding et al., 2017; Guan et al., 2019). However, there are obvious differences within the subduction-related belts, especially in the southern Okinawa Trough (Nakamura et al., 2003; Gao et al., 2006; Hao et al., 2006; Ding et al., 2017; Guan et al., 2019). Accordingly, an accurate reconstruction of the Moho topography in this region is necessary, and can be constrained from recently obtained datasets.

In this work, we integrate elevation and geoid anomaly data to determine the local isostatic Moho and lithosphere-asthenosphere

* Corresponding author.
E-mail addresses: sgjin@nuist.edu.cn, sg.jin@yahoo.com (S. Jin).

https://doi.org/10.1016/j.jseaes.2019.104098
Received 7 August 2019; Received in revised form 16 October 2019; Accepted 18 October 2019
Available online 22 October 2019

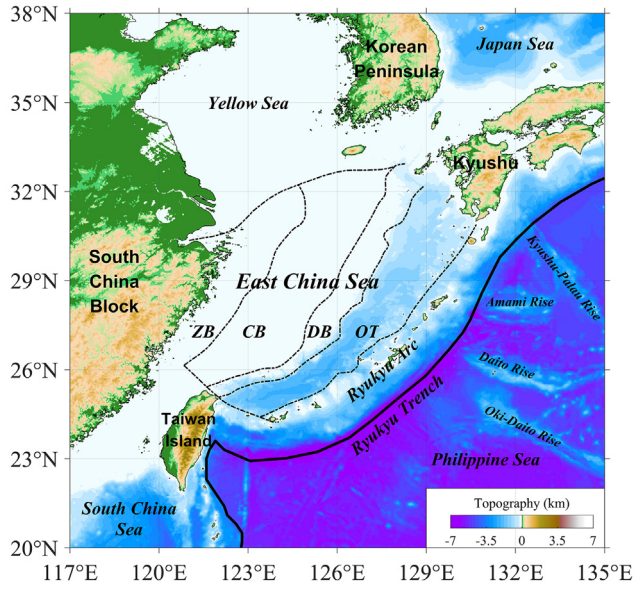

Fig. 1. Tectonic setting of the East China Sea and surroundings, with topography and bathymetry from ETOPO1. The thick black line is the boundary between the Eurasian and Philippine Sea Plates (Ryukyu Trench). The black dotted lines represent tectonic boundaries in the East China Sea. *ZB*, Zhe-Min uplift Belt; *CB*, Continental shelf Basin; *DB*, Diaoyudao uplift Belt; *OT*, Okinawa Trough.

boundary (LAB), and then invert the gravity Moho based on the complete Bouguer gravity anomaly. The vertical tectonic stress derived from the difference between the isostatic and gravity Moho is also presented, as well as discussion of the geodynamic implication for the ECS and surroundings.

2. Tectonic setting

The ECS is tectonically located between the South China Block and the Ryukyu Arc (Fig. 1). The neotectonics of the ECS is mainly constrained by the interactions among the Eurasian Plate, Pacific Plate and Philippine Sea Plate, in which the rifting currently plays an important role in kinematic interpretations (Kato et al., 1998; Sella et al., 2002; DeMets et al., 2010). The CB and DB started rifting in the Late Cretaceous (Yu and Chow, 1997; Xu et al., 2014) or Early Paleocene (Li et al., 2009) and, correspondingly, the rifting of the Okinawa Trough started in the Late Miocene to Early Pleistocene (Kimura, 1985; Sibuet et al., 1998), or in the Paleogene to Early Miocene (Xu et al., 2014). The progressive younging from the shoreline of mainland China to the Okinawa Trough (Ren et al., 2013; Suo et al., 2015) suggests that extension of the East Asian continent had occurred (Sibuet et al., 1998), along with the linkage of the Mesozoic evolution of the South China Block (Suo et al., 2015) and accounts for the differences in rifting history (Xu et al., 2014). The Okinawa Trough is the only active back-arc basin in the region, and was formed by extensional rifting along the continental marginal zone (Sibuet et al., 1998), which is in the early stage of evolution, as evidenced by recent geodetic observations (Sella et al., 2002; DeMets et al., 2010). East of the Okinawa Trough, the Ryukyu Arc is found parallel to the Okinawa Trough, and consists of a non-volcanic outer ridge and an inner volcanic front (Sibuet et al., 1998). Both the Okinawa Trough and Ryukyu Arc are constrained by the Taiwan Island to the southeast and Kyushu to the north, which led Bird (2003) to suggest that based on seismicity, this trough-arc system belongs to the same plate.

3. Methods

3.1. Estimation of the isostatic Moho and LAB depths

Generally, the isostatic Moho depth is estimated based on Airy's theory (Steffen et al., 2011; Fu et al., 2014; Fu and She, 2017). Using the elevation and geoid anomaly data, a two-layer model of the crust and lithospheric mantle, proposed by Fullea et al. (2006), is used to determine not only the Moho depth, but also the depth of the LAB under the assumption of local isostasy. It should be noted that the elasticity of the lithospheric mantle, as well as the average and vertical anomalous lithospheric density associated with the elevation and geoid anomaly (Doin and Fleitout, 1996; van Hees, 2000; Zeyen et al., 2005; Fullea et al., 2006) are considered in this method. Evidently, the isostatic Moho derived in this way is different from Airy's method.

In the present model, the rigid lithospheric columns are assumed to float on the inviscid liquid asthenosphere, and the pressure conforms to the lateral uniformity below the compensation level, z_{max}. The elevation, E, can be expressed as a function of the relationship between buoyancy and the lithospheric load (Lachenbruch and Morgan, 1990):

$$\begin{cases} E = \frac{\rho_a - \rho_L}{\rho_a} L - L_0 & (E \geq 0) \\ E = \frac{\rho_a}{\rho_a - \rho_w}\left(\frac{\rho_a - \rho_L}{\rho_a} L - L_0\right) & (E < 0) \end{cases} \quad (1)$$

and the average density of each lithospheric column, ρ_L, is:

$$\rho_L = \frac{(E + z_{ciso})\rho_c + (z_{Liso} - z_{ciso})\rho_m}{E + z_{Liso}} \quad (2)$$

where L is the total lithospheric thickness, L_0 is the asthenospheric level without lithospheric load [2400 m based on Zeyen et al. (2005) and Fullea et al. (2006)]; z_{ciso} and z_{Liso} are the isostatic Moho and LAB depths, and ρ_w, ρ_c, ρ_m and ρ_a are the densities of sea water, crust, lithosphere and asthenosphere, respectively. Substituting ρ_L from Eq. (2) into Eq. (1), the equation relating isostatic Moho and LAB depths (z_{ciso} and z_{Liso}) can be expressed as:

$$z_{ciso} = \frac{\rho_a L_0 + E(\rho_c - \rho_w) + z_{Liso}(\rho_m - \rho_a)}{\rho_m - \rho_c} \quad (3)$$

and $\rho_w = 0$ when $E > 0$.

Haxby and Turcotte (1978) used the formula

$$N = -\frac{2\pi G}{g} \int_z z \Delta\rho(z) dz \quad (4)$$

to calculate the geoid height N, given the density disturbances, $\Delta\rho(z)$, along a vertical profile. In Eq. (4), G is Newton's gravitational constant and g is gravitational acceleration (taken as 9.8 m/s^2 in this study). For the constant density distribution in the model of Fullea et al. (2006), the range of integration extends across a whole column above the compensation level. As such, Eq. (4) can be for the absolute densities of each layer:

$$N = -\frac{\pi G}{g}[\rho_w E^2 + (z_{ciso}^2 - E^2)\rho_c + (z_{Liso}^2 - z_{ciso}^2)\rho_m + (z_{max}^2 - z_{Liso}^2)\rho_a] - N_0 \quad (5)$$

The integration constant N_0 in Eq. (5) is used to adjust the zero level of the geoid anomaly, since the densities of each layer used in Eq.(5) are absolute values. The reference Moho and LAB depth (z_{c0} and z_{L0}) are applied in Eq. (5) to determine N_0. Given the densities of sea water, crust, lithospheric mantle and asthenosphere, the isostatic Moho and LAB depths (z_{ciso} and z_{Liso}) under local isostasy can be determined by combining Eqs. (3) and (5).

3.2. Parker-Oldenburg inversion method

The Parker-Oldenburg method is widely used for inversion of densities interfaces from gravity anomalies (Tirel et al., 2004; Steffen et al., 2011). Firstly, the gravity anomaly, $\Delta g(x,y)$, is linked to the undulation of the interface, $h(x,y)$, around the reference level, z_0, in the Fourier domain described by Parker (1973):

$$F[\Delta g(x,y)] = -2\pi G\Delta\rho e^{(-kz_0)}\sum_{n=1}^{\infty}\frac{k^{n-1}}{n!}F[h^n(x,y)] \quad (6)$$

where, $F[\ ]$ represents the Fourier transform and k is the wave vector of the transformed function, $\Delta\rho$ is the crust-mantle density contrast. Oldenburg (1974) deduced an iterative algorithm via modification of Eq. (6) as:

$$F[h(x,y)] = -\frac{F[\Delta g(x,y)]e^{(-kz_0)}}{2\pi G\Delta\rho} - \sum_{n=2}^{\infty}\frac{k^{n-1}}{n!}F[h^n(x,y)] \quad (7)$$

and the gravity-derived Moho depth, z_{cg}, is obtained as follow:

$$z_{cg} = z_0 + h(x,y) \quad (8)$$

For the iterative process convergence of Eq. (7), Oldenburg (1974) defined a filter

$$B(k) = \begin{cases} 1 & |k/2\pi| < WH \\ \frac{1}{2}\left[1+\cos\left(\frac{k-2\pi WH}{2(SH-WH)}\right)\right] & WH \leqslant |k/2\pi| \leqslant SH \\ 0 & |k/2\pi| > SH \end{cases} \quad (9)$$

The filter is used to restrict parts of the observations with high frequencies via the frequency parameters WH and SH.

Given the reference level, z_0, crust-mantle density contrast, $\Delta\rho$, and the cut-off frequencies (WH and SH), it is possible to compute the Moho relief, $h(x,y)$, versus the reference depth using Eq. (7) iteratively, and then obtain the gravity Moho depth, z_{cg}, using Eq. (8).

4. Data analysis and processing

The data used in this study, i.e. elevation, geoid anomaly and complete Bouguer gravity anomaly, are available in global datasets. Considering the potential boundary effects during the gravity calculation, all datasets were extended by 1 arc-degree in four directions based on the region shown in Fig. 1, meaning that the longitudinal and latitudinal range of 116–136°E and 19–39°N are used in the computations, respectively. The Earth Gravitation Model 2008 (EGM2008) dataset used in this study is a global dataset (Pavlis et al., 2008). As such, the same regular 5′×5′ grid is used in the elevation, geoid anomaly and gravity anomaly modeling.

4.1. Elevation and geoid anomaly

The elevation data, including topography and bathymetry, are from the ETOPO1 global database. The data have a vertical accuracy of approximately 10 m at best (Amante and Eakins, 2009), and cover elevation (in meters above mean sea level) approximately −7000 m in the Ryukyu Trench to > 3000 m on the Taiwan Island (Fig. 1). Offshore, the ocean depths are than 500 m in the Yellow Sea and western ECS, 500–1500 m in the Okinawa Trough, and 1500–3000 m in the South China Sea and Sea of Japan. In the Philippine Sea, the mean ocean depth exceeds 5000 m, but decreases to ~3000 m at four major oceanic rises. The average onshore topography is less than 1000 m in elevation, but locally exceeds 3000 m on the eastern side of Taiwan Island.

The geoid anomaly from the EGM2008 dataset is a spherical harmonic model (Pavlis et al., 2008) and varies from −11.5 m to 45.1 m referred the mean sea level (Fig. 2a). The NNE-SSW trending isolines characterize the study region and there is a significant local anomaly in the Ryukyu Arc enclosed by the 20 m contour line at the southwestern end of the arc. The other significant local anomaly is beneath Taiwan Island, reaching approximately 30 m.

To avoid any unrealistic effects in the depth model, the 1st, 2nd and 3rd order wavelet details of the elevation were filtered, which are the short wavelengths (< 100 km). Furthermore, Fullea et al. (2006) suggested that the long wavelengths of the geoid anomaly should be removed to avoid sharp cut-off effects. In our study, the 7th-order wavelet approximation of the geoid anomaly was removed, and the wavelengths of which are approximately 1400 km.

4.2. Bouguer gravity anomaly

The complete Bouguer gravity anomaly (Fig. 2b) is from World Gravity Map (WGM2012) with high-resolution of 2.5′ × 2.5′ (Bonvalot et al., 2012) and was computed at the Bureau Gravimétrique International. In this dataset, the terrain corrections have considered the contribution of most surface masses based on the ETOPO1 model, and the gravity effects of the sea-water, which contribute significantly to the surface mass in the oceanic region, have been corrected and are not needed again in further computation of the gravity anomaly.

4.2.1. Spectral analysis

Power spectral density (PSD) of the gravity anomaly is a powerful tool for determining the source depth and the wavelengths used for density-interface inversion (Spector and Grant, 1970), especially for determining the Moho depth (Shin et al., 2007; Steffen et al., 2011). We calculated the radial PSD of the Bouguer gravity anomaly, and a plot of PSD vs. wavenumber presents an exponential decrease (Fig. 3). According to the stepwise linear relation between the logarithmic PSD and the wavenumber, the reference levels at 162.8 km, 27.0 km and 3.8 km in Fig. 3 were estimated. The uncertainties of the linear fitting are 8.1 km, 1.6 km and 0.9 km, respectively. These reference levels are interpreted as follows: 162.8 km for LAB depth or subducting slabs (Hayes et al., 2018), 27.0 km for Moho depth and 3.8 km for the bottom depth of the sediments (Straume et al., 2019). In this work, we focus on determining the Moho depth using the wavenumber range of 0.003–0.008 km^{-1}, which is for fitting the 27.0 km reference level, as the spectral window for the gravity Moho inversion.

4.2.2. Gravity effects of the sediments

The thicknesses data of the sediments used in this study are from the recent global oceanic sediment thickness model GlobSed (Straume et al., 2019). Fig. 4a shows that the maximum sediment thickness exceeds 10 km in the northern CB, 7 km in the Sea of Japan and the northern South China Sea, 5 km in the Yellow Sea and 4 km in the southern CB. A sediment density of 2540 kg/m^3 is used to compute the gravity effects thereof, and the results (Fig. 4b) show approximate anomalies of −10 mGal in the Sea of Japan, Yellow Sea, ECS and South China Sea, and an anomaly of −40 mGal in the northern CB, where the high-profile Xihu depression occurs.

4.2.3. Gravity effects of the subducting slabs

Gravity anomaly features resulting from subducting slabs have been investigated in several previous studies, such as the African slab (Tirel et al., 2004; Grigoriadis et al., 2016). Because the depth of the Pacific slab is > 400 km beneath the study area (Liu et al., 2017; Hayes et al., 2018), its gravity effects are very limited and can thus be ignored. In this paper, the geometric parameters of the Ryukyu and Manila subducting slabs including depth and thickness (Fig. 5a and b) determined from the Slab2 model (Hayes et al., 2018) were adapted for slab-related corrections. The ~100 km thick Ryukyu slab reaches depths > 350 km, while a depth of 150 km is reached by the Manila slab (Fig. 5a), which is 80 km (Fig. 5b). The subduction direction of the Ryukyu slab is from ocean to the continent, while Manila slab subducts from continent to the ocean. During the computation of the gravity effects caused by the subducting slabs, the density contrasts of the ocean-continent

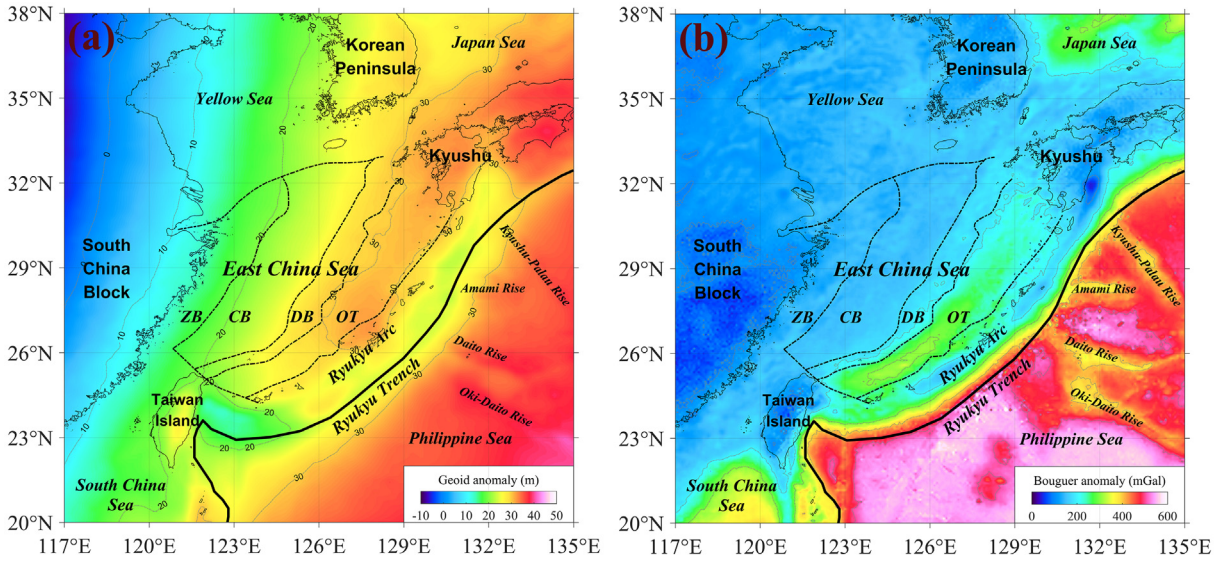

Fig. 2. (a) Geoid anomaly and (b) Bouguer gravity anomaly of the East China Sea. Abbreviations are as in Fig. 1.

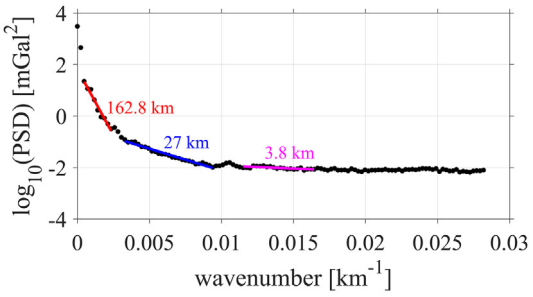

Fig. 3. Power spectral density (PSD) versus wavenumber of the Bouguer gravity anomaly. Note that three reference depths of 162.8 km, 27 km and 3.8 km were estimated from the linear relationship between the logarithmic PSD and the wavenumber.

lithospheres (10 kg/m^3) and lithosphere-asthenosphere (100 kg/m^3) were considered. Grigoriadis et al. (2016) used a unique density contrast of 55 kg/m^3 for the African subducting slab, since the slab is buried at a depth range of 90–250 km and mainly beneath the lithosphere. Fig. 5c shows the gravity effects induced by the subducting slabs. Along the Ryukyu slab, the positive anomaly exceeds 10 mGal, and dominates the wide region including the CB to the northwest and the Ryukyu Trench to the southeast. Notably, in the middle segment of the Okinawa Trough and Ryukyu Arc, the anomaly exceeds 60 mGal. The gravity effects of the Manila slab reach a value of −30 mGal at the east margin of the South China Sea.

4.2.4. Corrected gravity anomaly

The surface mass, including the land and ocean, has to be taken into account during computation of the complete Bouguer gravity anomaly. Therefore, after removing the gravity effects of the sediments and subducting slabs (Figs. 4b and 5c) from the complete Bouguer gravity anomaly (Fig. 2b), a corrected gravity anomaly is obtained (Fig. 6), which mainly reflects variations in the Moho depth.

5. Results and analysis

5.1. Isostatic Moho and LAB depths

According to the seismic study of Cho et al. (2011) and spectral analysis of the Bouguer gravity anomaly (Fig. 3), the reference depths

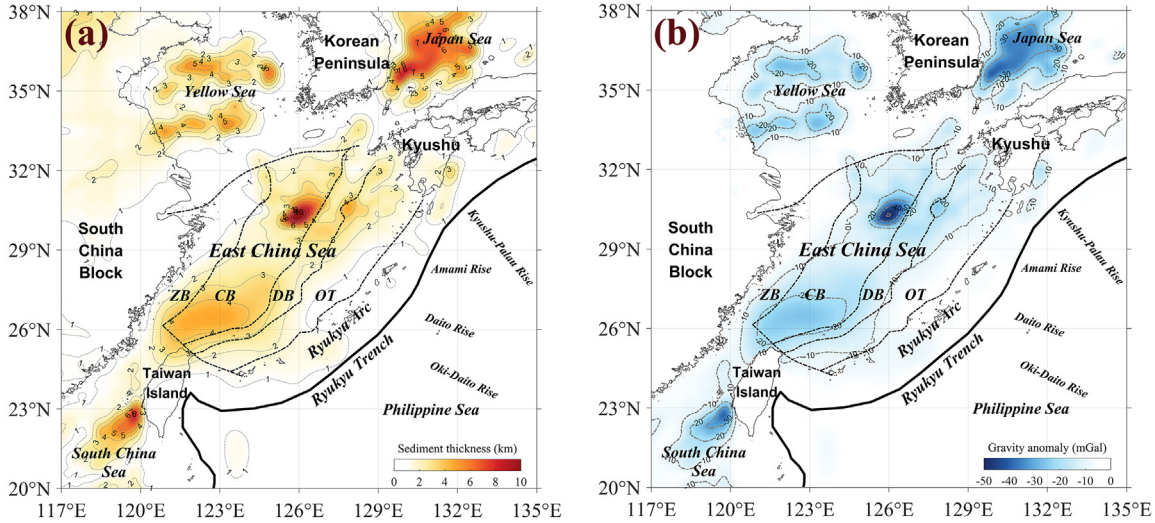

Fig. 4. (a) Map of sediment thickness and (b) its gravity effects in the East China Sea. Abbreviations are as in Fig. 1.

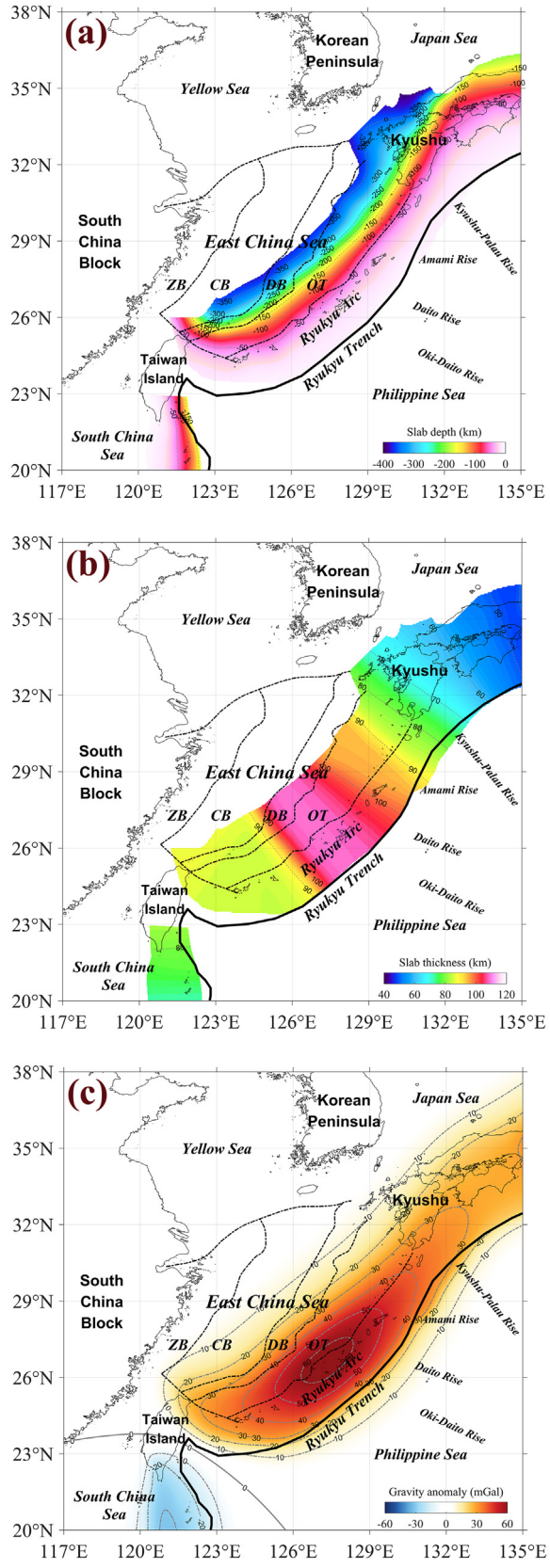

Fig. 5. Geometry of the subducting slabs and their gravity effects. (a) Slab depth beneath the East China Sea, (b) thickness of the Ryukyu and Manila subducting slabs and (c) gravity effects of the subducting slabs. Abbreviations are as in Fig. 1.

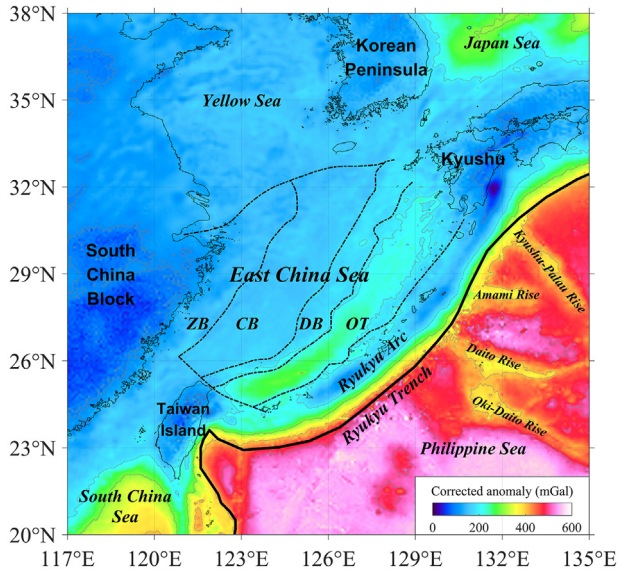

Fig. 6. Corrected gravity anomaly after removing the gravity effects of the sediments (Fig. 4b) and subducting slabs (Fig. 5c) from the Bouguer gravity anomaly (Fig. 2b). Abbreviations are as in Fig. 1.

Table 1
Parameters used in estimation of the isostatic Moho and LAB.

Parameter	Symbol	Value
Sea-water density	ρ_w	1030 kg/m^3
Crustal density	ρ_c	2670 kg/m^3
Lithospheric mantle density	ρ_m	3300 kg/m^3
Asthenospheric density	ρ_a	3200 kg/m^3
Depth of compensation level	z_{max}	300 km
Reference of Moho depth	z_{c0}	27 km
Reference of LAB depth	z_{L0}	120 km

of the Moho (27 km) and LAB (120 km) were chosen. Although the densities of the continental and oceanic crust are different, a homogeneous density of 2670 kg/m^3 was chosen based on Guy et al. (2017). The other parameters required for estimation of the isostatic Moho and LAB are presented in Table 1.

Fig. 7a shows that the shallow isostatic Moho is at a depth of ~15 km in the Philippine Sea, except for the oceanic rises where depths are 15–20 km. The depth increases abruptly towards the west, northwest and north, reaching 38 km below the Taiwan Island, > 25 km in the Ryukyu Arc and ~35 km beneath Kyushu. In the ECS and Yellow Sea, the isostatic Moho is in the depth range of 24–30 km at the Okinawa Trough to the southeast and ~32 km near the coastlines to the west. Along the boundary of the DB and Okinawa Trough, the isostatic Moho varies by ~6 km across a narrow zone, and then presents smooth lateral variations from east to west. In the southern Okinawa Trough, the Moho depth is 24–28 km, while it is ~30 km in the northern Okinawa Trough. The thickened crust with an isostatic Moho depth of ~35 km presents beneath Taiwan Island, the South China Block and the North China Craton (north of ~32°N in mainland China). In the South China Sea and Sea of Japan, the isostatic Moho depths are in the 19–25 km and 27–30 km range, respectively.

The isostatic LAB shown in Fig. 7b indicates thin lithosphere (120 km) in the Philippine Sea, while deeper LAB (120–140 km) occurs in the Ryukyu Arc, especially near Japan, where depth exceeds140 km. LAB depths of 110–120 km occur in the southern Okinawa Trough and ~120 km in the northern Okinawa Trough. The LAB beneath Taiwan Island, the Korean Peninsula and the Sea of Japan occurs at depths of ~125 km. In the western ECS (CB and ZB), Yellow Sea and onshore of mainland China, the LAB gradually increases in depth from east to west,

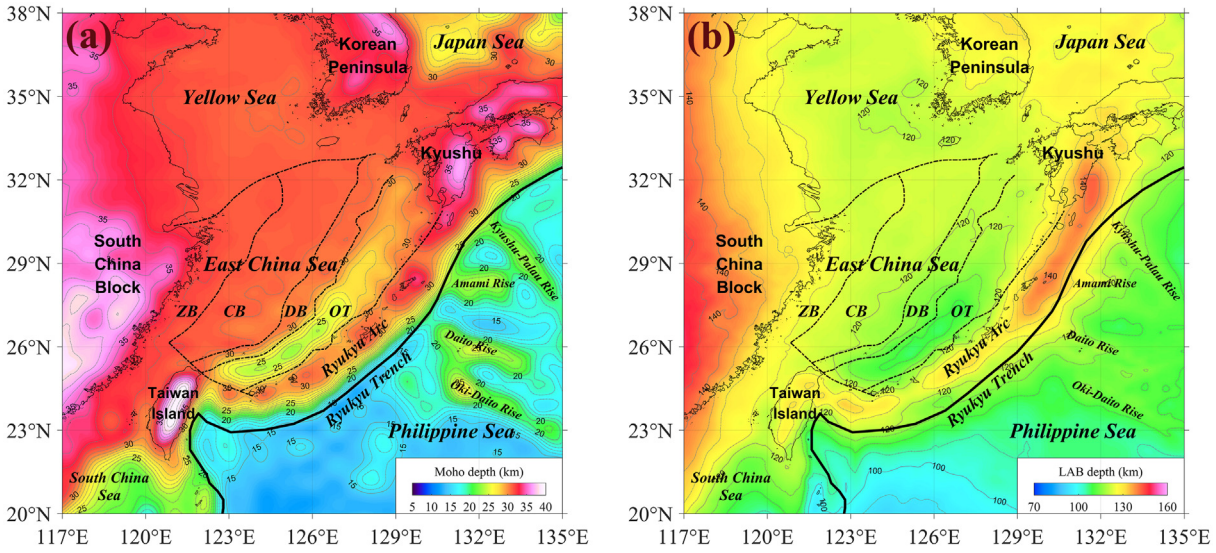

Fig. 7. Depth of the local isostatic (a) Moho and (b) lithosphere-asthenosphere boundary (LAB). Abbreviations are as in Fig. 1.

reaching ~150 km to the west.

5.2. Gravity Moho depth

5.2.1. Density contrast

The reference Moho depth of 27 km has been determined by spectral analysis, and the density contrast between crust and mantle is another parameter required for gravity inversion. The seismic Moho depth (Fig. 8) is from the CRUST1.0 model (Laske et al., 2013) and is used here to compare it with that from our gravity inversion result. The crust-mantle density contrast is varied from 400 to 700 kg/m^3 and the reference Moho depth is varied from 20 to 35 km for gravity inversion. Fig. 9a shows the root-mean-square (RMS) results between Moho depths of 20–35 km in the whole study region, suggesting an RMS minimum of 4.5 km where the reference depth is 23.5 km and the density contrast is 550 kg/m^3. When the reference depth is 27 km and the density contrast is 550 kg/m^3, RMS is 5.6 km. The region within the geographic window of 116–126°E and 29–39°N was selected for calculating RMS, because the Moho variations are relatively smooth in this region. Fig. 9b shows that RMS is < 3 km when the density contrast is in the range of 500–700 kg/m^3 and the reference depth is ~27 km. For a density contrast of 550 kg/m^3, the RMS is 2.6 km. To be definitive but maintain generality, a density contrast of 550 kg/m^3 was used for the gravity inversion. This agrees with the density contrast between granite in the crust and peridotite in the lithospheric mantle (Brocher, 2005).

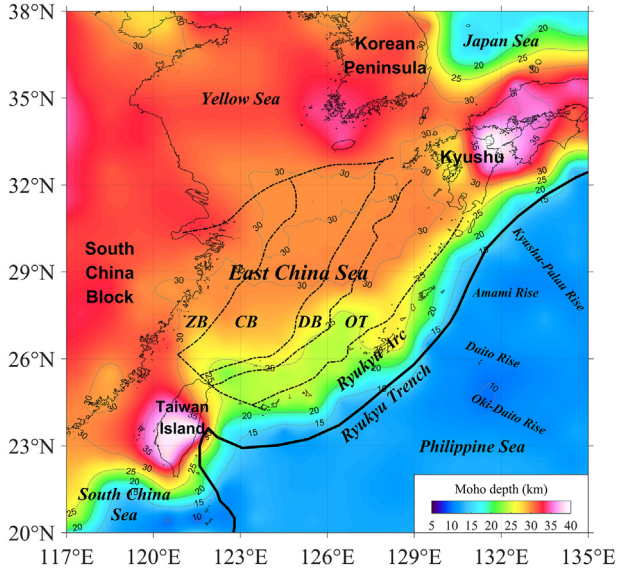

Fig. 8. Moho depth from the CRUST1.0 (Laske et al., 2013). Abbreviations are as in Fig. 1.

5.2.2. Moho topography

After three iterations using the Parker-Oldenburg method mentioned above, the inversion results (Fig. 10) are obtained with an RMS of 0.017 mGal. Fig. 10a presents the Moho from gravity inversion and its gravity effect is shown in Fig. 10b. The difference between the corrected and calculated gravity anomalies is presented in a 2D image (Fig. 10c) and distribution histogram (Fig. 10d). The residuals with a mean of 0 mGal and standard deviation (σ) of 48.98 mGal follow a normal distribution where 87.35%, 92.96% and 96.52% of the residuals are < 1σ, 2σ and 3σ, respectively. The significant residuals are distributed in the Ryukyu and Manila subduction zones, as well as four oceanic rises in the Philippine Sea.

The features of the gravity Moho are basically consistent with the isostatic Moho (Fig. 7a), but different from that of the CRUST1.0 (Fig. 8) at the Ryukyu Trench and Arc, the Manila subduction zone and oceanic rises. This may result from the lower spatial resolution of the CRUST1.0 model.

The gravity Moho depth varies from 5.3 km in the Philippine Sea to 38.1 km at the eastern margin of Kyushu. In the Philippine Sea, the Moho is at a depth of ~15 km except in the region of the four oceanic rises where the mean depth is ~20 km. The southern part of the Ryukyu subduction zone is a remarkable area with sharp depth variations; deepening by ~20 km from the Ryukyu Trench to the Ryukyu Arc, and then rising by ~10 km from the Ryukyu Arc to the Okinawa Trough. Compared to the neighboring DB and Ryukyu Arc, the southern Okinawa Trough has a locally uplifted Moho belt with depths of 25–30 km. In the other units of the ECS and Yellow Sea, the Moho occurs at ~31 km with no significant variation. The other region with significant depth variation (~10 km) is beneath Taiwan Island and the Manila subduction zone. The deeper Moho is extensive beneath Taiwan Island and reaches a depth of ~37 km. In the Manila subduction zone, the Moho varies from 25 to 30 km depth at the west margin to 15–20 km at the east margin. The coastal zone of the South China block also represents a gradient of the Moho depth variation, with an increase of 5 km from ~31 km in the ZB to ~36 km in the South China Block. The Moho is shallow beneath the South China Sea and Sea of Japan,

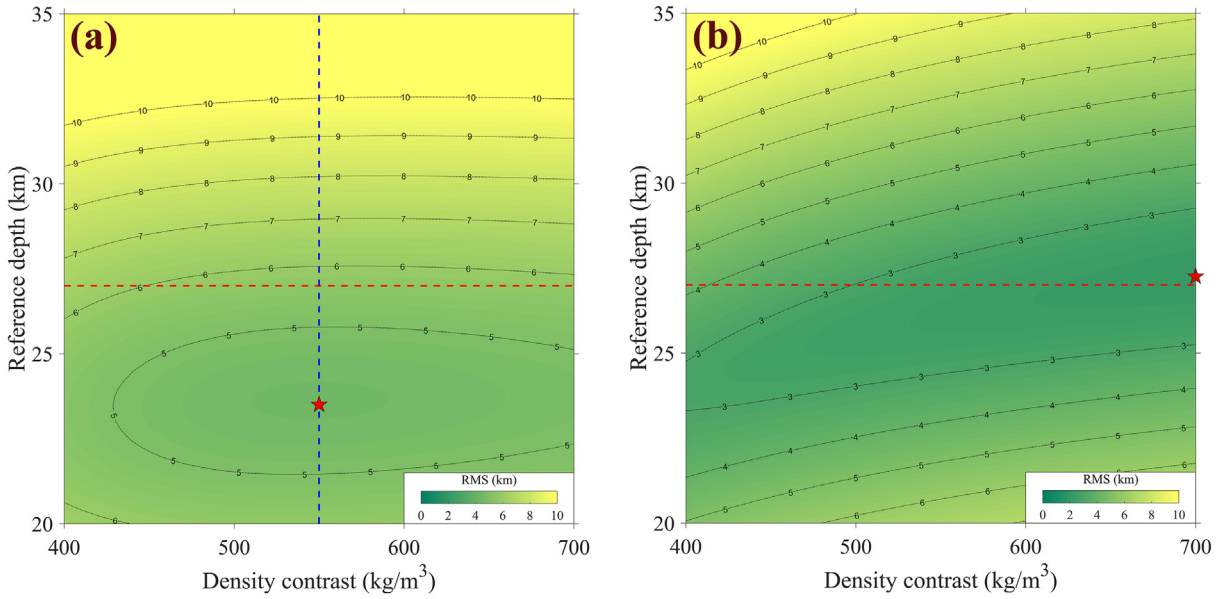

Fig. 9. Root-mean-square (RMS) results between the Moho depth determined from gravity inversion and from the CRUST1.0 model. (a) RMS in the whole region and (b) RMS in the geographic window of 116–126°E and 29–39°N. The red stars mark the RMS minimum in each panel. The red dashed lines denote the reference depth of 27 km determined by spectral analysis. The blue dashed line denotes the density contrast of 550 kg/m^3, which is considered as the density contrast for gravity inversion.

occurring at depths of ~20 km and ~25 km, respectively.

6. Discussion

6.1. Gravity Moho compared with previous studies

Our gravity Moho (Fig. 10a) mostly agrees with profiles obtained from deep seismic sounding (Teng et al., 2013) and seismic tomography (Ma et al., 2018), as well as the Curie points from magnetic estimates of the ECS (Lin et al., 2005). However, our gravity Moho is ~5 km deeper than some previous results derived from gravity inversion under the DB, Okinawa Trough and Ryukyu Arc (Hao et al., 2006; Ding et al., 2017; Guan et al., 2019). Without the gravity effects of the subducting slabs (Fig. 5c), it is expected that the gravity Moho should be shallower under the Ryukyu subduction zone and deeper under the Manila subduction zone. By transferring a gravity anomaly of 40–60 mGal to the Moho level using the empirical Bouguer formula, the depth changes by 2–3 km, which therefore suggests that the above differences mainly result from the gravity effects of the Ryukyu subducting slab.

6.2. Isostatic state of the crust

The isostatic and gravity Moho presented in this work are both associated with the gravity field of the Earth. The isostatic Moho related to the geoid anomaly can be used to infer the depth of crustal compensation (Haxby and Turcotte, 1978; van Hees, 2000; Fullea et al., 2006), while the gravity Moho derived from the Bouguer gravity anomaly ideally indicates undulation of the "true" Moho (Hao et al., 2006; Shin et al., 2007; Steffen et al., 2011; Guy et al., 2017). Direct comparison between the isostatic and gravity Moho is generally used to indicate the isostatic stage of the crust (Steffen et al., 2011; Fu et al., 2014). The most significant difference between the isostatic and gravity Moho is evident in the Ryukyu trench-arc system as it differs by −5 to 8 km, suggesting a state of non-isostatic equilibrium of the crust.

Alternatively, according to the relation between crustal load and buoyancy of the lithosphere, the positive and negative vertical tectonic stresses (VTS) can be considered representative of the respective upward and downward motion of the crust that is being subjected isostatic adjustment (Gao et al., 2016; Fu and She, 2017; Guy et al., 2017). The VTS, P_{vertical}, is calculated by the following equation: $P_{\text{vertical}} = (z_{cg} - z_{ciso})(\rho_m - \rho_c)g$ (e.g. Gao et al., 2016), where the parameters are as above. The VTS results in this work (Fig. 11) show a negative VTS belt along the northwest margin of the Philippine Sea, including the Ryukyu Trench, and a positive VTS beneath the Ryukyu Arc. Stresses of < 10 MPa occur in most of the ECS, Yellow Sea and South China Block, thus indicating isostatic balance. The negative VTS values imply that the area is undercompensated at crustal level and has an overall downwards vertical movement in the crust, which is in agreement with the subduction of the Philippine Sea Plate. In contrast, the positive crustal load in the Ryukyu Arc inferred from the positive VTS values indicates crustal overcompensation and upward motion. If the rifted ECS (Li et al., 2009; Xu et al., 2014), especially the Okinawa Trough (Kimura, 1985; Sibuet et al., 1998), is presently a tensional structure as indicated from geodetic observations (Sella et al., 2002; DeMets et al., 2010), then the positive load will likely balance gradually. It should be noted that there is a distinct negative VTS value of > 10 MPa beneath the eastern edge of Taiwan Island.

6.3. Crustal structures and geodynamics from the Moho topography

Several geodynamic models had been proposed to interpret the rift of the ECS since the Late Cretaceous and the origin of the Okinawa Trough. Although lithospheric thermal expansion has not been taken into account, the gravity Moho (Fig. 10a) is mostly consistent with that of Bai et al. (2014) under the northeastern South China Sea. The gravity Moho shows a decrease in depth from the South China Block to the DB, an uplifting-subsiding structure across the Okinawa Trough and Ryukyu Arc and an abrupt slope between the Ryukyu Arc and Philippine Sea. There is also the thin oceanic crust in the Philippine Sea evident in the profile-view of Fig. 12b–d and 3D view in Fig. 13. An analysis of crustal thickness (sum of elevation and Moho depth) or basement thickness (removing the sediment thickness from crustal thickness, Fig. 14), perhaps, will make a broader comparison. In view of the thick sediments (Fig. 4a) overlying relatively thin basement (Fig. 14), the scenario is consistent with subsiding sub-basins in the ECS. For example, there is locally thin basement of < 25 km in the northern CB (Fig. 12c, 12g and 14) which corresponds to the Xihu depression (Li et al., 2009). Moreover, two thin E-W-trending basement belts in the Yellow Sea

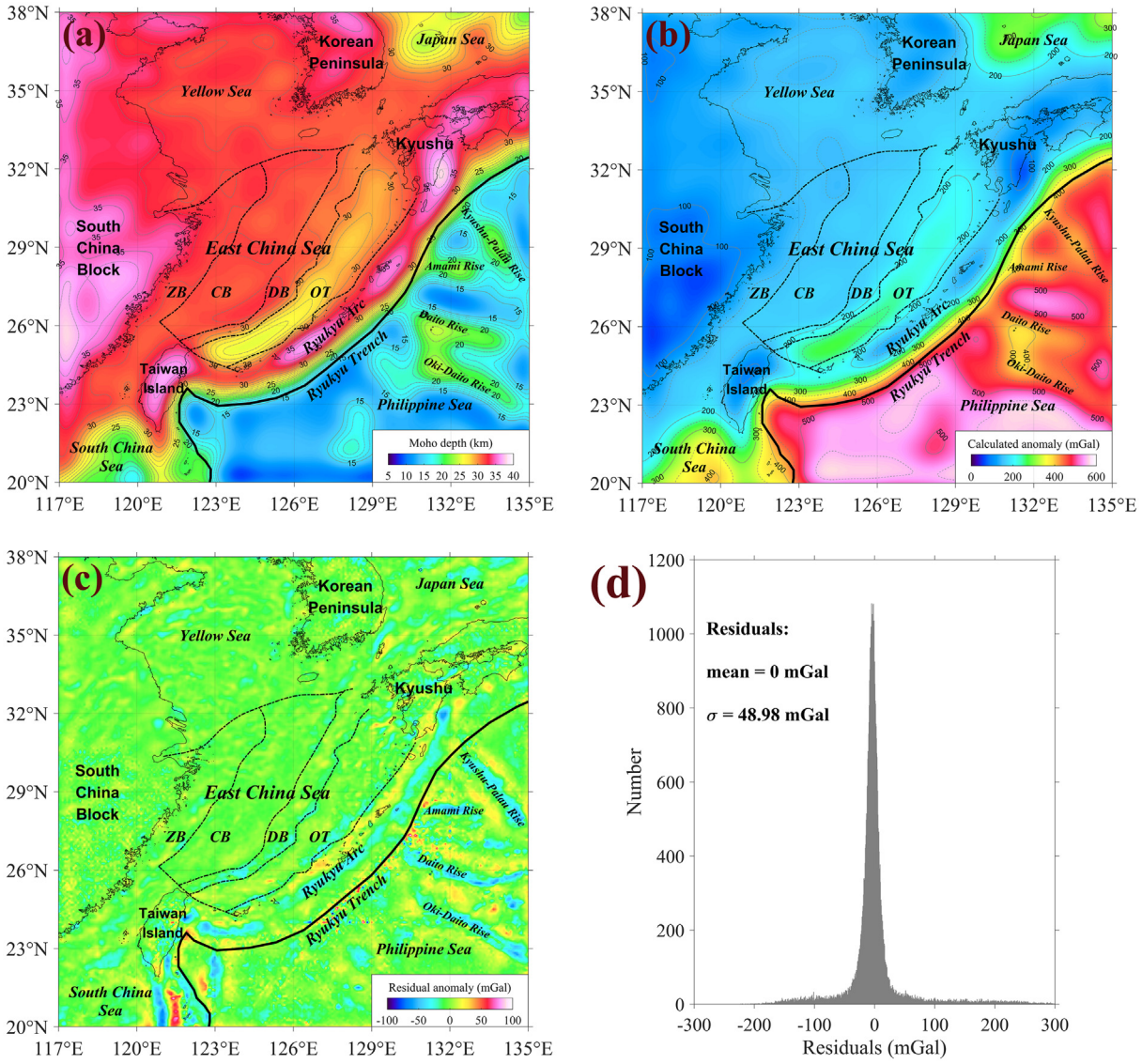

Fig. 10. Results of the gravity inversion. (a) Moho depth. (b) Calculated anomaly from Moho depth shown in (a). (c) Residual anomaly map between corrected anomalies shown in Fig. 6 and calculated anomaly shown in (b). (d) Distribution histogram of the residuals shown in (c) indicating a mean of 0 mGal. Abbreviations are as in Fig. 1.

(Fig. 14) also agree with the presence of basins in the south and north Yellow Sea, as presented in previous work (Choi et al., 2015). As such, the resulting gravity Moho presented here appears to characterize quite well the crustal structure, and can be used to at least partially evaluate the evolution of the ECS.

The isostatic and gravity Moho depth (Fig. 7a and 10a) of ~30 km under the ZB, CB and DB is consistent with that of sub-continental crust, which is similarly evident beneath the Yellow Sea. With the exception of the boundary between the DB and Okinawa Trough, the tectonic faults defined by geological studies (Xu et al., 2014; Suo et al., 2015; Shang et al., 2017) are not reflected in our gravity Moho, and the tectonic units ZB, CB and DB cannot be distinguished clearly. This suggests that the properties of the crustal structure behave very similarly at the scale of the whole crust. Indeed, this can also be deduced by the lack of change in the relatively low temperature of ~600 °C at the Moho level (Wang and Cheng, 2012). Some authors, such as Ding et al. (2017), argued that the CB is an allochthonous terrain which collided with the South China Block in the Late Cretaceous. However, it is difficult to recognize the remnant suture between the ZB and CB in the whole crust from our Moho models or from the seismic structures (Feng et al., 1993; Gao et al., 2006; Hao et al., 2006; Liu et al., 2017). Accordingly, we suggest that the origin of the ECS is related to the extension of the Eurasian continent, which accords with Xu et al. (2014) and Suo et al. (2015).

The abrupt changes in gravity Moho depth occur in the Okinawa Trough, Ryukyu Arc and Ryukyu Trench from west to east or southeast (Fig. 10a), which is also a region of pronounced VTS (Fig. 11). It is straightforward to observe that the tilting direction and angle of the Moho accords with the subduction direction of the slabs in both profile (Fig. 12) and in 3D view (Fig. 13), suggesting that the sharp Moho changes correspond with the subducting slabs. It is worth noting that the Moho in the Okinawa Trough is distinctly shallower than in the western ECS (including the ZB, CB and DB), which is likely the result of the difference in rifting history (Xu et al., 2014). When considering the vertical movements of the Ryukyu Arc and Trench inferred from the VTS results (Fig. 11), the Okinawa Trough should still be a recent rifting structure, which has been revealed by geological and geodetic research (Kimura, 1985; Yu and Chow, 1997; Kato et al., 1998; Sella et al., 2002). It is expected that this would have been steeper under the comprehensive function of eastward extension of the ECS, subduction

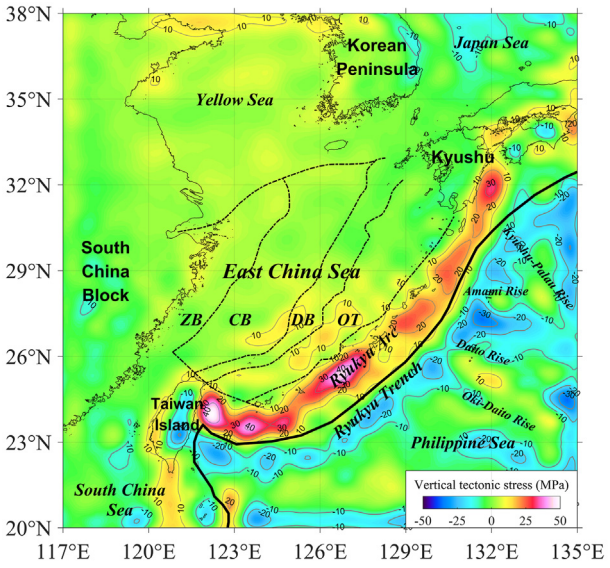

Fig. 11. Map showing the vertical tectonic stress in the crust in the East China Sea and surroundings. Abbreviations are as in Fig. 1.

of the Philippine Sea Plate and isostatic compensation. In addition, the same Ryukyu slab is subducting beneath the southern ECS from two directions (Fig. 12b); this reveals different patterns of the Moho undulation from subduction, which accords with the W- and E-class subduction zone proposed by Harabaglia and Doglioni (1998). The shallower Moho (Fig. 10a) and thinner basement (Fig. 14) might be related to the twin subduction directions of the Ryukyu slab, thus implying that the southern Okinawa Trough might be spreading faster than the northern Okinawa Trough (Xu et al., 2014; Shang et al., 2017).

7. Conclusions

The undulations of the isostatic and gravity Moho in the ECS and surroundings have been estimated from the available global datasets (e.g. ETOPO1 and WGM2012). Recent models of sediments and subducting slabs (GlobSed and Slab2) were used for gravity corrections during gravity inversion. After isostatic analysis, the Moho models provide some new information about the crustal structures and geodynamics of the ECS region.

The Moho model characterize a decrease in Moho depth from the ZB to DB, a buckled morphology across the Okinawa Trough, Ryukyu Arc and Trench from west to east, and steep uplift along the Ryukyu Trench. Under the western ECS, including the ZB, CB and DB, the Moho has a similar depth to the continental pattern, which is supported by evidence that this marginal sea is resulted from extension of the Eurasian continent. Consequently, the shallow Moho of the Okinawa Trough, which locates between the deep Moho of the western ECS and Ryukyu Arc, implies that the Okinawa Trough is a crustal rifting structure. The sharp change in the Moho depth along the Ryukyu Trench might be related to the subduction of the Philippine Sea Plate, which has a shallow Moho. Finally, evaluation of the crustal isostatic state by comparing the isostatic and gravity Moho reveals that mainland China, the ECS and the Yellow Sea are the compensated regions, and the Moho of the overcompensated Ryukyu Arc should subsequently become uplifted, while the undercompensated Ryukyu Trench should become depressed.

Declaration of Competing Interest

The authors declare that they have no known competing financial interests or personal relationships that could have appeared to influence the work reported in this paper.

Acknowledgements

This work was supported by the National Key Research and

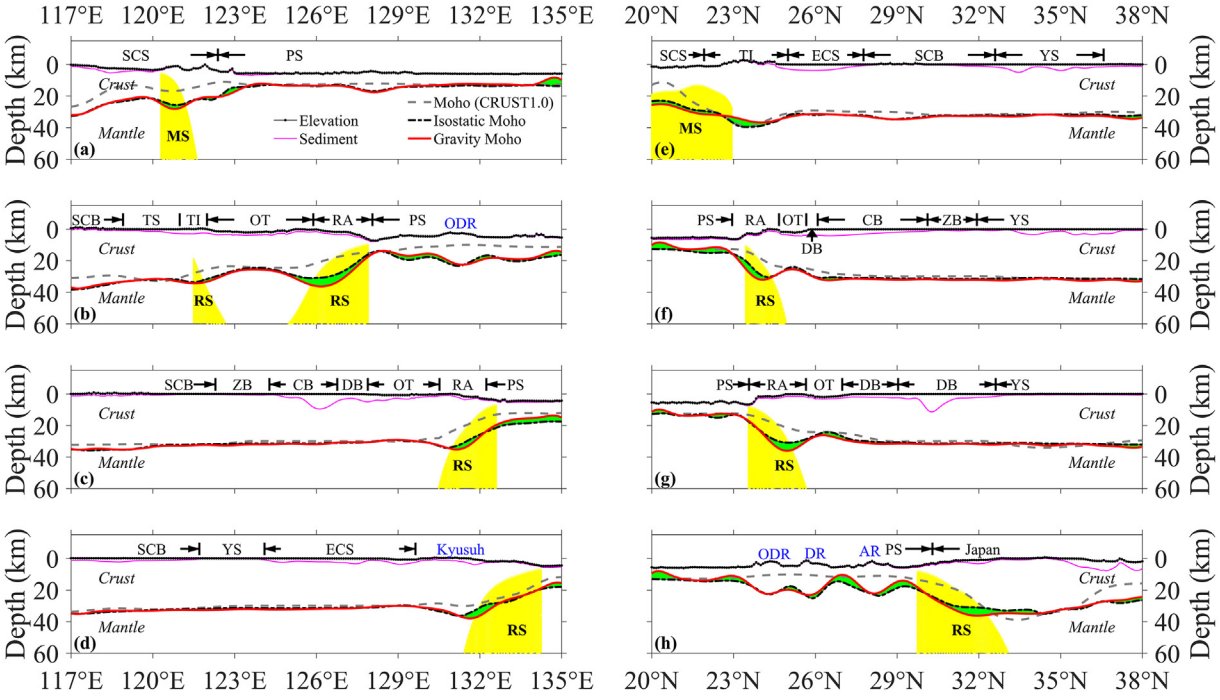

Fig. 12. (a–d) Depth profiles for 21, 25, 30.5 and 32°N, and (e–h) depth profiles for 121, 124, 126 and 132°E. Yellow shading indicates the subducting slabs (Manila slab; MS and Ryukyu slab; RS). The depth differences between isostatic and gravity Moho depths are shaded green. *SCS*, South China Sea; *PS*, Philippine Sea; *SCB*, South China Block; *TS*, Taiwan Strait; *TI*, Taiwan Island; *RA*, Ryukyu Arc; *YS*, Yellow Sea; *ESC*, East China Sea; *KP*, Korean Peninsula; *ODR*, Oki-Daito Rise; *KPR*, Kyushu-Palau Rise; *DR*, Daito Rise; *AR*, Amami Rise. Other abbreviations are as in Fig. 1.

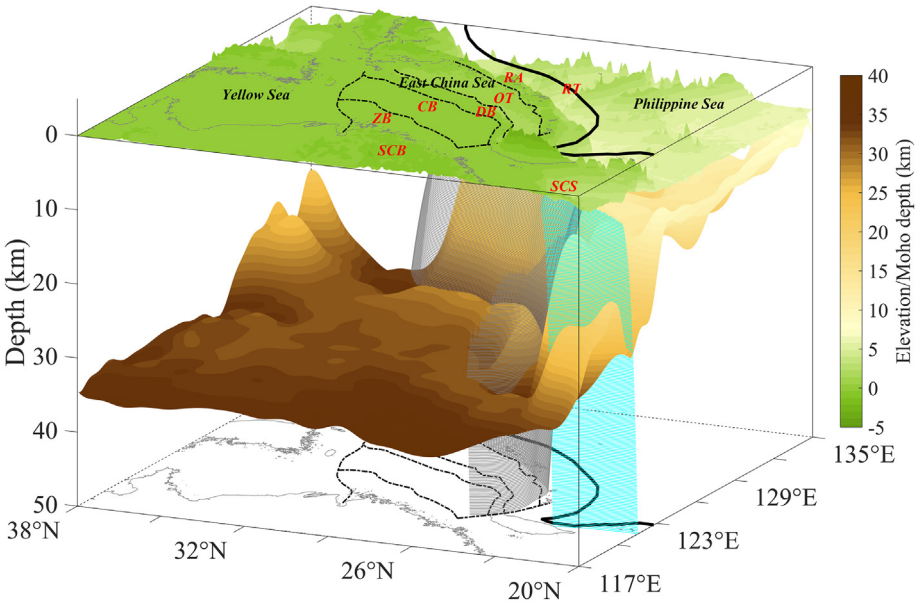

Fig. 13. 3D view of topographic elevation and Moho depth. The gray and cyan shades denote the upper boundaries of the Ryukyu and Manila subducting slabs. *RA*, Ryukyu Arc; *RT*, Ryukyu Trench; *SCB*, South China Block; *SCS*, South China Sea. Other abbreviations are as in Fig. 1.

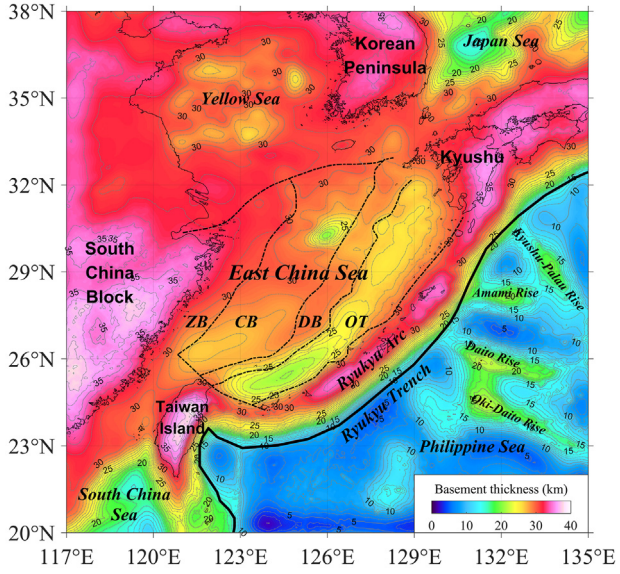

Fig. 14. Basement thickness map derived from the gravity Moho depth (Fig. 10a), elevation (Fig. 1) and thickness of sediments (Fig. 4a). Abbreviations are as in Fig. 1.

Development Program of China Project (Grant No. 2018YFC0603502), Startup Foundation for Introducing Talent of NUIST (Grant No. 2243141801036), and Jiangsu Province Distinguished Professor Project (Grant No. R2018T20). We thank Warwick Hastie, PhD, from Liwen Bianji, Edanz Group China (www.liwenbianji.cn/ac), for editing the English text of a draft of this manuscript.

Appendix A. Supplementary material

Supplementary data to this article can be found online at https://doi.org/10.1016/j.jseaes.2019.104098.

References

Amante, C., Eakins, B.W., 2009. ETOPO1 1 Arc-Minute Global Relief Model: Procedures, Data Sources and Analysis, NOAA Technical Memorandum NESDIS NGDC-24. National Geophysical Data Center, NOAA.

Autin, J., Scheck-Wenderoth, M., Gotze, H.J., Reichert, C., Marchal, D., 2016. Deep structure of the Argentine margin inferred from 3D gravity and temperature modelling, Colorado Basin. Tectonophysics 676, 198–210.

Bai, Y.L., Williams, S.E., Muller, R.D., Liu, Z., Hosseinpour, M., 2014. Mapping crustal thickness using marine gravity data: Methods and uncertainties. Geophysics 79, G27–G36.

Bird, P., 2003. An updated digital model of plate boundaries. Geochems. Geophys. Geosyst. 4 (3), 1027. https://doi.org/10.1029/2001GC000252.

Bonvalot, S., Balmino, G., Briais, A., Kuhn, M., Peyrefitte, A., Vales, N., Biancale, R., Gabalda, G., Reinquin, F., Sarrailh, M., 2012. World Gravity Map. In: BGI-CGMW-CNES-IRD (Ed.), Commission for the Geological Map of the World, Paris.

Brocher, T.A., 2005. Empirical relations between elastic wavespeeds and density in the earth's crust. Bull. Seismol. Soc. Am. 95, 2081–2092.

Cho, K.H., Chen, H.W., Kang, I.B., Lee, S.H., 2011. Crust and upper mantle structures of the region between Korea and Taiwan by surface wave dispersion study. Geosci. J. 15, 71–81.

Choi, S., Ryu, I.C., Gotze, H.J., 2015. Depth distribution of the sedimentary basin and Moho undulation in the Yellow Sea, NE Asia interpreted by using satellite-derived gravity field. Geophys. J. Int. 202, 41–53.

DeMets, C., Gordon, R.G., Argus, D.F., 2010. Geologically current plate motions. Geophys. J. Int. 181, 1–80.

Ding, W., Li, J., Wu, Z., Li, S., Lin, X., 2017. Late Mesozoic transition from Andean-type to Western Pacific-type of the East China continental margin—Is the East China Sea basement an allochthonous terrain? Geological J. 53 (5), 1994–2002.

Doin, M.-P., Fleitout, L., 1996. Geoid anomalies and the structure of continental and oceanic lithospheres. J. Geophys. Res. 101, 16119–16135.

Feng, R., Zhou, H.N., Yao, Z.S., Ma, G.M., Li, Q.L., 1993. 3D velocity structure and its tectonic implications in the East China Sea and Yellow Sea. Acta Geol. Sin. 6 (3), 273–296.

Fu, G.Y., Gao, S.H., Freymueller, J.T., Zhang, G.Q., Zhu, Y.Q., Yang, G.L., 2014. Bouguer gravity anomaly and isostasy at western Sichuan Basin revealed by new gravity surveys. J. Geophys. Res. Solid Earth 119, 3925–3938.

Fu, G.Y., She, Y.W., 2017. Gravity anomalies and isostasy deduced from new dense gravimetry around the Tsangpo Gorge. Tibet. Geophys. Res. Lett. 44, 10233–10239.

Fullea, J., Fernàndez, M., Zeyen, H., 2006. Lithospheric structure in the Atlantic-Mediterranean transition zone (southern Spain, northern Morocco): a simple approach from regional elevation and geoid data. Comptes Rendus Geoscience 338, 140–151.

Gao, D.Z., Zhao, J.H., Bo, Y.L., Tang, J., 2006. A study on lithosphere 3D structure in the East China Sea and adjacent regions. Chinese J. Geol. 41 (1), 10–26 (in Chinese with English abstract).

Gao, S.H., She, Y.W., Fu, G.Y., 2016. A new method for computing the vertical tectonic stress of the crust by use of hybrid gravity and GPS data. Chinese J. Geophys. 59, 2006–2013 (in Chinese with English abstract).

Grigoriadis, V.N., Tziavos, I.N., Tsokas, G.N., Stampolidis, A., 2016. Gravity data inversion for Moho depth modeling in the Hellenic area. Pure Appl. Geophys. 173, 1223–1241.

Guan, D.L., Ke, X.P., Wang, Y., 2019. Effective elastic thickness of the lithosphere in the East and South China Seas and adjacent area obtained using the convolution method. J. Asian Earth Sci. 175, 247–255.

Guy, A., Holzrichter, N., Ebbing, J., 2017. Moho depth model for the Central Asian

Orogenic Belt from satellite gravity gradients. J. Geophys. Res. Solid Earth 122, 7388–7407.
Hao, T.Y., Xu, Y., Xu, Y., Mancheol, S., Liu, J.H., Dai, M.G., Li, Z.W., 2006. Some new understanding on deep structure in Yellow Sea and East China Sea. Chinese J. Geophys. 49, 458–468 (in Chinese with English abstract).
Harabaglia, P., Doglioni, C., 1998. Topography and gravity across subduction zones. Geophys. Res. Lett. 25, 703–706.
Haxby, W.F., Turcotte, D.L., 1978. On isostatic geoid anomalies. J. Geophys. Res. 83, 5473–5478.
Hayes, G.P., Moore, G.L., Portner, D.E., Hearne, M., Flamme, H., Furtney, M., Smoczyk, G.M., 2018. Slab2, a comprehensive subduction zone geometry model. Science 362, 58–61.
Jin, S.G., Park, P., Zhu, W., 2007. Micro-plate tectonics and kinematics in Northeast Asia inferred from a dense set of GPS observations. Earth Planet. Sci. Lett. 257 (3–4), 486–496. https://doi.org/10.1016/j.epsl.2007.03.011.
Kato, T., Kotake, Y., Nakao, S., Beavan, J., Hirahara, K., Okada, M., Hoshiba, M., Kamigaichi, O., Feir, R.B., Park, P.H., Gerasimenko, M.D., Kasahara, M., 1998. Initial results from WING, the continuous GPS network in the western Pacific area. Geophys. Res. Lett. 25, 369–372.
Kimura, M., 1985. Back-arc rifting in the Okinawa Trough. Marine Petrol. Geol. 2, 222–240.
Lachenbruch, A.H., Morgan, P., 1990. Continental extension, magmatism, and elevation Formal relations and rules of thumb. Tectonophysics 174, 39–62.
Laske, G., Masters., G., Ma, Z., Pasyanos, M., 2013. Update on CRUST1.0 - A 1-degree Global Model of Earth's Crust. Geophys. Res. Abstracts 15, Abstract EGU2013-2658.
Li, C.F., Zhou, Z., Ge, H., Mao, Y., 2009. Rifting process of the Xihu Depression, East China Sea Basin. Tectonophysics 472, 135–147.
Li, Z.X., Li, X.H., Chung, S.L., Lo, C.H., Xu, X.S., Li, W.X., 2012. Magmatic switch-on and switch-off along the South China continental margin since the Permian: Transition from an Andean-type to a Western Pacific-type plate boundary. Tectonophysics 532, 271–290.
Lin, J.Y., Sibuet, J.C., Hsu, S.K., 2005. Distribution of the East China Sea continental shelf basins and depths of magnetic sources. Earth Planets Space 57, 1063–1072.
Liu, X., Zhao, D.P., Li, S.Z., Wei, W., 2017. Age of the subducting Pacific slab beneath East Asia and its geodynamic implications. Earth Planet. Sci. Lett. 464, 166–174.
Ludwig, W.J., Murauchi, S., Den, N., Buhl, P., Hotta, H., Ewing, M., Asanuma, T., Yoshii, T., Sakajiri, N., 1973. Structure of East China Sea-West Philippine Sea Margin off southern Kyushu, Japan. J. Geophys. Res. 78, 2526–2536.
Ma, J.C., Tian, Y., Liu, C., Zhao, D.P., Feng, X., Zhu, H.X., 2018. P-wave tomography of Northeast Asia: constraints on the western Pacific plate subduction and mantle dynamics. Phys. Earth Planet. Int. 274, 105–126.
Nakamura, M., Yoshida, Y., Zhao, D.P., Katao, H., Nishimura, S., 2003. Three-dimensional P- and S-wave velocity structures beneath the Ryukyu arc. Tectonophysics 369, 121–143.
Oldenburg, D.W., 1974. The inversion and interpretation of gravity anomalies. Geophysics 39, 526–536.
Parker, R.L., 1973. The rapid calculation of potential anomalies. Geophys. J. R. Astr. Soc. 31, 447–455.
Pavlis, N.K., Holmes, S.A., Kenyon, S.C., Factor, J.K., 2008. An Earth gravitational model to degree 2160: EGM2008, EGU General Assembly. European Geosciences Union, Vienna, Austria.
Ren, J.S., Niu, B.G., Wang, J., Jin, X.C., Zhao, L., Liu, R.Y., 2013. Advances in research of Asian geology–A summary of 1:5M International Geological Map of Asia project. J. Asian Earth Sci. 72, 3–11.
Sella, G.F., Dixon, T.H., Mao, A.L., 2002. REVEL: A model for Recent plate velocities from space geodesy. J. Geophys. Res. Solid Earth 107, B4. https://doi.org/10.1029/2000JB000033.
Shang, L.N., Zhang, X.H., Jia, Y.G., Han, B., Yang, C.-S., Geng, W., Pang, Y.M., 2017. Late Cenozoic evolution of the East China continental margin: Insights from seismic, gravity, and magnetic analyses. Tectonophysics 698, 1–15.
Shin, Y.H., Xu, H., Braitenberg, C., Fang, J., Wang, Y., 2007. Moho undulations beneath Tibet from GRACE-integrated gravity data. Geophys. J. Int. 170, 971–985.
Sibuet, J.C., Deffontaines, B., Hsu, S.K., Thareau, N., Le Formal, J.P., Liu, C.S., Party, A., 1998. Okinawa trough backarc basin: Early tectonic and magmatic evolution. J. Geophys. Res. Solid Earth 103, 30245–30267.
Spector, A., Grant, F.S., 1970. Statistical models for interpreting aeromagnetic data. Geophysics 35, 293–302.
Steffen, R., Steffen, H., Jentzsch, G., 2011. A three-dimensional Moho depth model for the Tien Shan from EGM2008 gravity data. Tectonics 30, TC5019. https://doi.org/10.1029/2011tc002886.
Straume, E.O., Gaina, C., Medvedev, S., Hochmuth, K., Gohl, K., Whittaker, J.M., Abdul Fattah, R., Doornenbal, J.C., Hopper, J.R., 2019. GlobSed: Updated total sediment thickness in the world's oceans. Geochem. Geophys. Geosyst. 20, 1756–1772.
Suo, Y.H., Li, S.Z., Zhao, S.J., Somerville, I.D., Yu, S., Dai, L.M., Xu, L.Q., Cao, X.Z., Wang, P.C., 2015. Continental margin basins in East Asia: tectonic implications of the Meso-Cenozoic East China Sea pull-apart basins. Geol. J. 50, 139–156.
Teng, J.W., Zhang, Z.J., Zhang, X.K., Wang, C.Y., Gao, R., Yang, B.J., Qiao, Y.H., Deng, Y.F., 2013. Investigation of the Moho discontinuity beneath the Chinese mainland using deep seismic sounding profiles. Tectonophysics 609, 202–216.
Thybo, H., Artemieva, I.M., Kennett, B., 2013. Moho: 100 years after Andrija Mohorovičić. Tectonophysics 609, 1–8.
Tiberi, C., Diament, M., Lyon-Caen, H., King, T., 2001. Moho topography beneath the Corinth Rift area (Greece) from inversion of gravity data. Geophys. J. Int. 145, 797–808.
Tirel, C., Gueydan, F., Tiberi, C., Brun, J.P., 2004. Aegean crustal thickness inferred from gravity inversion. Geodynamical implications. Earth Planet. Sci. Lett. 228, 267–280.
van Hees, G.L.S., 2000. Some elementary relations between mass distributions inside the Earth and the geoid and gravity field. J. Geodyn. 29, 111–123.
Wang, Y., Cheng, S.H., 2012. Lithospheric thermal structure and rheology of the eastern China. J. Asian Earth Sci. 47, 51–63.
Xu, J.Y., Ben-Avraham, Z., Kelty, T., Yu, H.S., 2014. Origin of marginal basins of the NW Pacific and their plate tectonic reconstructions. Earth-Sci. Rev. 130, 154–196.
Yu, H.S., Chow, J., 1997. Cenozoic basins in northern Taiwan and tectonic implications for the development of the eastern Asian continental margin. Palaeogeogr. Palaeocl. 131, 133–144.
Zeyen, H., Ayarza, P., Fernandez, M., Rimi, A., 2005. Lithospheric structure under the western African-European plate boundary: A transect across the Atlas Mountains and the Gulf of Cadiz. Tectonics 24, TC2001. https://doi.org/10.1029/2004tc001639.